IOPscience iopscience.iop.org

Home Search Collections Journals About Contact us My IOPscience

Monte Carlo simulations of the recombination dynamics in porous silicon

This article has been downloaded from IOPscience. Please scroll down to see the full text article.

1996 J. Phys.: Condens. Matter 8 5161

(http://iopscience.iop.org/0953-8984/8/28/003)

View the table of contents for this issue, or go to the journal homepage for more

Download details:
IP Address: 171.66.16.206
The article was downloaded on 13/05/2010 at 18:18

Please note that terms and conditions apply.

J. Phys.: Condens. Matter **8** (1996) 5161–5187. Printed in the UK

Monte Carlo simulations of the recombination dynamics in porous silicon

H Eduardo Roman† and Lorenzo Pavesi‡

† Institut für Theoretische Physik, Universität Giessen, Heinrich-Buff-Ring 16, D-35392 Giessen, Germany

‡ INFM and Dipartimento di Fisica, Università di Trento, via Sommarive 14, I-38050 Povo (Trento), Italy

Received 1 February 1996, in final form 1 May 1996

Abstract. A simple lattice model describing the recombination dynamics in visible-light-emitting porous silicon is presented. In the model, each occupied lattice site represents a Si crystal of nanometre size. The disordered structure of porous silicon is modelled by modified random percolation networks in two and three dimensions. Both correlated (excitons) and uncorrelated electron–hole pairs have been studied. Radiative and non-radiative processes as well as hopping between nearest-neighbour occupied sites are taken into account. By means of extensive Monte Carlo simulations, we show that the recombination dynamics in porous silicon is due to a dispersive diffusion of excitons in a disordered arrangement of interconnected Si quantum dots. The simulated luminescence decay for the excitons shows a stretched exponential lineshape while for uncorrelated electron–hole pairs a power-law decay is suggested. Our results successfully account for the recombination dynamics recently observed in experiments. The present model is a prototype for a larger class of models describing diffusion of particles in a complex disordered system.

1. Introduction

Silicon, the most studied semiconductor, is not a good light emitter, especially in the visible range, because of its indirect-band-gap transition in the infrared (1.1 eV). The recently discovered optical properties of porous forms of silicon (porous Si) have therefore attracted considerable interest [1, 2, 3, 4]. In addition to the internal nanometre-sized structures which are distributed in space according to a complex topology [5], these new materials have similar spectral behaviours, the most prominent of which are a rather high luminescence quantum efficiency and an unexpectedly wide range of luminescence lifetimes (ranging from microseconds to milliseconds), depending on temperature.

The mechanism of the luminescence emission is still unclear. Three main models have been proposed and are still under debate:

(i) the quantum recombination model [6, 7, 8];
(ii) the surface-state model [9]; and
(iii) the molecular recombination model [10, 11, 12].

The first two models agree on the fact that the energy spectrum of porous Si is a result of the quantum confinement of carriers in Si nano-crystals. Still under debate is the shape of the nano-crystal that has been described either in terms of ‘undulating’ quantum wires [6] or quantum dots [8]. The quantum recombination and the surface-state models differ in their

0953-8984/96/285161+27$19.50 © 1996 IOP Publishing Ltd

predictions about the origin of the luminescence. In the first case, the luminescence is due to confined *and* localized excitons, while in the second, the luminescence is due to electron–hole pair recombination, where the electron and the hole could be found either in a bulk nano-crystal state (an 'extended' state), or being trapped into a surface nano-crystal state (a 'localized' state). The third model, the molecular recombination model, considers that some particular molecular species like polysilane chains (e.g. the SiH chain [10]) or siloxene-like rings (Si–O–H) [11] form on the surface of the Si nano-crystals. The luminescence is due to the carrier trapping into these species.

Recent experiments [13–20] have provided clear evidence of anomalous relaxation behaviour of the luminescence. The decay lineshape, for a *single* observation energy, is *not* described by a single exponential function. This non-exponential behaviour is commonly described by a stretched exponential function [21, 22, 23], defined as

$$L(t) = L(0)\exp[-(t/\tau)^{\beta}] \tag{1}$$

where $L(t)$ is the time-dependent luminescence intensity, τ is a lifetime and $\beta \leqslant 1$ a dispersion exponent. In general, values of $\beta < 1$ correspond to the existence of a broad distribution of lifetimes. In some circumstances, such broad distributions may be the result of a diffusive motion of the excited carriers. This may be the case in porous Si, as suggested recently in terms of trap-controlled hopping processes [18]. We elaborate this idea further in this work.

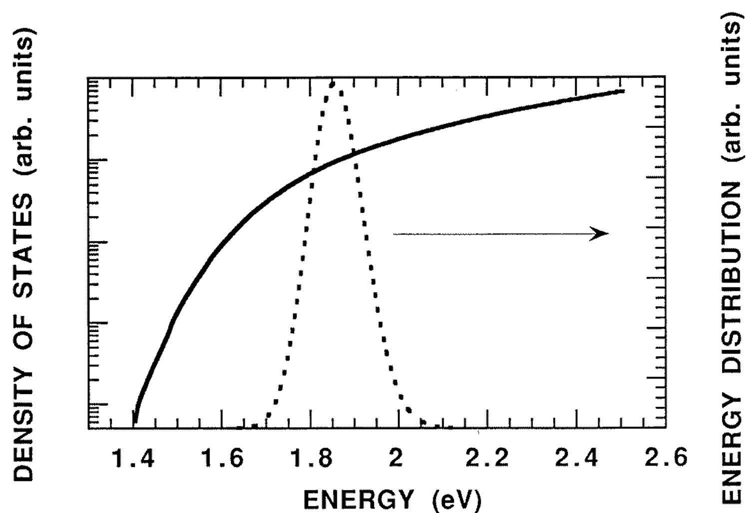

Figure 1. The distribution of optical band-gaps for an ensemble of quantum dots (dotted line) (equation (2)), and the corresponding density of states (continuous line) (equation (4)) versus energy.

Motivated by these experimental results, and by the fact that little is known about the recombination dynamics of the charge carriers in these materials, we have initiated a detailed numerical study of the underlying transport behaviour in porous Si by means of Monte Carlo (MC) simulations.

In this work, we present a simple model of porous Si in which nanometre-sized crystals (nano-crystals), characterized by a distribution of radiative and non-radiative recombination times, are assumed to be randomly placed at the sites of percolation-like clusters defined

on square and simple cubic lattices. Charge carriers are allowed to hop between nearest-neighbour occupied cluster sites. The competing effect between radiative and non-radiative transitions in a single Si nano-crystal, as well as the effects of geometrical constraints on hopping of carriers due to the complex topology of percolation clusters, are discussed.

Even though our simulations are based on the quantum recombination model [6, 7], they are consistent with other possible recombination mechanisms because the model concentrates on the dynamics of the recombination and not on the recombination process itself. However, we found that most of the data are better explained by our simulations when the quantum recombination model is assumed. In addition, since our model is based on quite general assumptions about the geometrical disorder involved, we expect that it may be applied to a larger class of physical systems characterized by both a structural and local disorder, of which porous Si is just one possible example.

The paper is organized as follows: in section 2 the model is described, and exact solutions obtained in the case of isolated Si nano-crystals are discussed. In sections 3 and 4, simulation results for one-, and two- and three-dimensional systems, respectively, are presented. In section 5, a discussion of the present results is presented and they are compared to other results already known in the literature. Finally, in section 6 we give some concluding remarks.

2. The model for Si nanometre-sized crystals

We consider a lattice model for porous Si in which occupied and empty sites are present. Each occupied site of the lattice represents a Si nano-crystal. In one dimension, all the sites are occupied by Si nano-crystals, while in higher dimensions the occupied sites are randomly distributed in space and interconnected to each other according to the topology of percolation-like clusters (see section 4). We further assume that the physical properties, relevant for our problem, of such Si nano-crystals are suitably described in terms of quantum dots (QD), for which many theoretical results are currently available.

2.1. The size and radiative energy of a Si nano-crystal

Each Si nano-crystal, or equivalently, each occupied site of the lattice, is characterized by a size d, representing its mean diameter (typically in the range 15 to 55 Å [24]). Since the actual spatial distribution of nano-crystal sizes is not known *a priori*, the sizes d_i at sites i are chosen randomly according to a Gaussian distribution $P(d)$ [25]. We used $P(d) \sim (1/\sigma_d)\exp[-(1/2\sigma_d^2)(d-d_0)^2]$, centred at $d_0 = 32.4$ Å and having a width $\sigma_d = 0.8$ Å. For simplicity, we further assume that the underlying (hypercubic) lattice has a lattice constant $a \cong d_0$, which determines the unit of length used in our calculations.

In one dimension, this *local* randomness is the only source of disorder in the model, while in higher dimensions, an additional (geometrical) disorder, due to the complex structure of percolation-like clusters, is also present (see section 4).

Due to the experimental method of preparation of porous Si, however, some correlation between the sizes d may actually be present for nearby Si nano-crystals, from which one may reasonably expect that strong local variations in d are not likely to occur [5]. To take this effect into account in a simple way, the sizes d corresponding to nearest-neighbour occupied sites are not allowed to differ by more than a pre-fixed amount. We are going to specify this point below.

By neglecting the excitonic binding energy, the optical band-gap energy E associated with a given Si nano-crystal is assumed to correspond to the emission energy determined

experimentally. E_i is related to the size d_i through the power-law relation recently suggested on the basis of calculations performed for spherical quantum dots [26]. Based on these calculations, we assume $E_i = E_0(d_0/d_i)^n$, with $n \cong 1.39$, where $E_0 = 1.86$ eV is the transition energy for a Si nano-crystal of size d_0. The corresponding distribution for E is then of the form

$$P(E) \sim \frac{1}{\sigma_d} \frac{1}{E^{1+1/n}} \exp[-(d_0^2/2\sigma_d^2)((E_0/E)^{1/n} - 1)^2] \qquad (2)$$

centred around E_0 and having a width at half-maximum of about 0.16 eV (see figure 1).

It is instructive to obtain estimates of the total density of states $\rho(\epsilon)$ resulting from these distributions. For simplicity, an ensemble of quantum dots of cubic shape and side $L_x = L_y = L_z = d$ is considered [27]. The (confined) electronic states have energies $\epsilon(n_{x,y,z}) = \epsilon_0(n_x + n_y + n_z)$, where $\epsilon_0 = \hbar^2\pi^2/(2\mu d^2)$, n_x, n_y and n_z are the principal quantum numbers for motion in the x, y and z directions, $n_{x,y,z} \geqslant 1$ and μ represents the effective mass of the exciton. In this simple model, we have neglected the binding energy of the exciton and assumed that the effective mass of the hole is much larger than that of the electron. Then, the transition energy E can be related to the ground-state energy of the QD by $E = 3\epsilon_0 + E_{\mathrm{Bulk}}$, where $E_{\mathrm{Bulk}} = 1.15$ eV is the bulk Si indirect gap. The density of states for a single quantum dot of size d with an energy barrier of height $V(\mathrm{QD})$ is then [27]

$$\rho_d(\epsilon) \cong \frac{2V(\mathrm{QD})}{d^3} \sum_{n_{x,y,z}} \delta(\epsilon - \epsilon(n_{x,y,z}) - E_{\mathrm{Bulk}}) \qquad (3)$$

where ϵ is an energy and the total density of states is

$$\rho(\epsilon) = \sum_d P(d)\rho_d(\epsilon). \qquad (4)$$

This quantity is plotted in figure 1 assuming a Gaussian broadening of the single QD state of 0.01 eV. The density of states of an ordered ensemble of QDs should reveal a series of distinct peaks corresponding to the different confined states $\epsilon(n_{x,y,z})$ in the QD. The random Gaussian distribution of sizes, yielding a distribution of E, smears out the discrete peaks and yields an approximately exponential behaviour of the form $\rho(\epsilon) \sim \exp(\epsilon/\epsilon_a)$, with $\epsilon_a \cong 0.35$ eV, at large ϵ.

To deal with the above-mentioned spatial correlations in d, the difference in energy between nearest-neighbour sites i and j, $\Delta E_{ij} = E_j - E_i$, is allowed to take absolute values smaller than a given cut-off E_{cut}. This is the criterion employed to accept a given value of d_j, with respect to the previous value at site i, from the Gaussian distribution. In dimensions higher than one, this criterion is applied simultaneously with the growing process (see section 4). For convenience, we consider variations in energy, rather than variations in size to select the values of the local quantities E and d. The results are not sensitive to this choice. Typical calculations have been performed for values in the range $10^{-4} < E_{\mathrm{cut}} < 0.4$ eV (see section 3).

2.2. The radiative and non-radiative recombination times

Within each Si nano-crystal, both radiative and non-radiative recombination processes occur when excited electron–hole pairs are present. Both processes depend on the size d of the nano-crystal.

The emission process is assumed to be due to excitonic recombinations in a QD. In this case, it was shown that the radiative recombination time, τ_{rad}, results from the thermal

balance between the occupation of the exchange-split singlet and triplet excitonic states [7],

$$\tau_{\rm rad}(E,T) = \tau_{\rm tripl}\left[\frac{1+(1/3)\exp(-\Delta E_x/k_BT)}{1+(1/3)(\tau_{\rm tripl}/\tau_{\rm sing})\exp(-\Delta E_x/k_BT)}\right]. \tag{5}$$

$\tau_{\rm sing}$ (the radiative lifetime for the singlet excitonic state) is obtained from the values calculated in [28]:

$$\tau_{\rm sing}(E) = \tau_{\rm sing}^{(0)}\left(\frac{E_{\rm Bulk}}{E-E_{\rm Bulk}}\right)^{n_{\rm s}} \tag{6}$$

where $n_{\rm s} = 1.5$. At the present, no theoretical calculations are available for the radiative lifetime of the triplet excitonic state, $\tau_{\rm tripl}$. Thus, $\tau_{\rm tripl}$ is estimated from the experimental data reported in [7]:

$$\tau_{\rm tripl}(E) = \tau_{\rm tripl}^{(0)}[\tau_{\rm sing}(E)]^{\alpha_{\rm s}} \tag{7}$$

where $\tau_{\rm tripl}^{(0)} = 2368\ \mu$s, and $\alpha_{\rm s} = 0.307$.

Finally, the quantum-confinement-enhanced exchange energy $\Delta E_x = E_x^{Si}(d_x/d)^3$, where $E_x^{Si} = 3.165\times 10^{-4}$ eV is the exchange energy in crystalline Si and $d_x = 43$ Å, is obtained from the calculations in [29].

Non-radiative recombinations have been considered as multiphonon transition processes for trapping on a deep centre [30], for which the non-radiative recombination time, $\tau_{\rm nr}$, is given by

$$\tau_{\rm nr}(T) = \tau_{\rm nr}^{(0)}\frac{{\rm e}^{2n_TS}}{(n_T+1)^p} \tag{8}$$

where $n_T = [\exp(\hbar\omega_{ph}/k_BT)-1]^{-1}$ is the density of phonons with energy $\hbar\omega_{ph}$, and S and p are related to the details of the capturing centre. Here we have used nano-crystal size-independent quantities, with $\hbar\omega_{ph}/k_B = 800$ K, $S = 1$, and $p = 25$. If bulk Si optical phonons are involved, $\hbar\omega_{ph}/k_B \simeq 1100$ K; lower values can be justified by the typical softening of the phonon modes in a confined system on a localized centre.

It should be emphasized that the actual nature and origin of non-radiative phonon transition processes in porous Si nano-crystals remain to be understood. Here, such processes are included because they certainly play a very important role in the recombination dynamics of carriers [8, 9]. The form for $\tau_{\rm nr}$ in equation (8) can be only considered as a first approximation to the actual form of the non-radiative recombination time, yet it is expected to describe the physics involved correctly, at least in a qualitative fashion. In this work, the same $\tau_{\rm nr}$ has been employed for all the Si nano-crystals.

2.3. The rates of hopping between Si nano-crystals

In addition to the internal structure of Si nano-crystals, hopping of electrons, holes and excitons may actually occur between nearby nano-crystals. To describe the diffusion of carriers in porous Si, we consider hopping processes only between nearest-neighbour (n.n.) occupied sites of the lattice for two different models. In the first model, only one type of carrier hops, representing the exciton, while in the second, two different types of carrier can hop, representing the electron and hole. If the electron and hole (e–h) motions are strongly correlated, e.g. if the hole closely follows the electron as it moves in the system, one has essentially the first model. As we will see in sections 3 and 4, a qualitatively different behaviour is obtained when e–h hops are completely uncorrelated. In both models, correlated and uncorrelated e–h pairs, the on-site radiative recombination is assumed to be excitonic.

The rates of transition for a carrier of type x ($x \equiv$ ex, representing the exciton, $x \equiv$ e, the electron, and $x \equiv$ h, the hole) from the site i to its nearest-neighbour occupied site j are defined as

$$P_{ij}^x = \frac{1}{\tau_{\rm hop}^x} \qquad \text{when } E_j - E_i \leqslant 0 \tag{9}$$

and

$$P_{ij}^x = \frac{1}{\tau_{\rm hop}^x} \exp(-f_x\, \Delta E_{ij}/k_B T) \qquad \text{when } E_j - E_i \geqslant 0 \tag{10}$$

where $\Delta E_{ij} = E_j - E_i$. When the site j is not occupied, as may occur in two- and three-dimensional systems, then $P_{ij}^x = 0$. Here, $0 < f_x \leqslant 1$ is an additional parameter related to the band structure of nano-crystals, and $\tau_{\rm hop}^x$ is a characteristic time for tunnelling of x-carriers between nearby (n.n.) Si nano-crystals, which is temperature independent. In equations (9) and (10), no dependence on the intersite distance, r_{ij}, between n.n. Si nano-crystals is explicitly shown. In a more refined version of the present model, one could consider in equations (9) and (10) a dependence on r_{ij} of the form

$$\frac{1}{\tau_{\rm hop}^x} = \nu_x \exp(-\gamma_{ij} r_{ij}) \tag{11}$$

where ν_x is an attempt frequency and γ_{ij} is related to the energy barrier which separates the QDs at sites i and j. The quantities γ_{ij} and r_{ij} may then be considered as random variables. For simplicity, we use $\tau_{\rm hop}^x = \tau_{\rm hop}$ here, independently of the type of carrier. Thus, the dependence of hopping rates on x is only contained in the factor f_x.

Table 1. Values used in the Monte Carlo calculations. $\ell^{(3/D)}$ is the linear size of the D-dimensional lattice employed, $t_{\rm max}$ the maximum number of MC steps for a single run, $n_{\rm runs}$ the number of runs (i.e. the number of different particles used) for a single cluster realization, and $n_{\rm conf}$ the number of different cluster realizations over which the reported results are averaged. The meaning of the other parameters is given in the text. All of the results presented in this paper refer to this choice of parameters unless otherwise stated.

ℓ	$t_{\rm max}$	$n_{\rm runs}$	$n_{\rm conf}$	$\tau_{\rm hop}$	$\tau_{\rm sing}^{(0)}$	$n_{\rm s}$	$\tau_{\rm nr}^{(0)}$	$\hbar\omega_{\rm ph}/k$	p	Porosity	$E_{\rm cut}$
31	4000	2000	200	150 μs	150 μs	1.5	900 μs	800 K	25	65 %	0.04 eV

In our calculations, we have arbitrarily chosen $f_{\rm e} = 1/3$, $f_{\rm h} = 2/3$ and $f_{\rm ex} = 0.4$ in order to take into account the distribution of the energy-gap discontinuity, $E - E_{\rm Bulk}$, among the valence and conduction bands [31]. Extensive Monte Carlo simulations have been done by using the same set of parameters but for different $f_{\rm ex}$. The effect of varying $f_{\rm ex}$ is to change the barrier for hopping, $f_{\rm ex}\, \Delta E_{ij}$, which is mostly relevant at low temperatures. By increasing $f_{\rm ex}$, a decrease in the luminescence decay rate occurs, but essentially no changes in the luminescence decay lineshapes are observed, i.e. in equation (1) τ increases and β remains constant. The mean distances over which the excitons move before recombination are reduced as the effective barrier, $f_{\rm ex}\, \Delta E_{ij}$, is increased. However, for $f_{\rm ex}$ in the interval [0.2–0.6] the numerical results are qualitatively not affected and quantitatively they change by less than 10%. Table 1 reports the values of all of the parameters used in our simulations for 1D, 2D and 3D systems whose results are presented in the following.

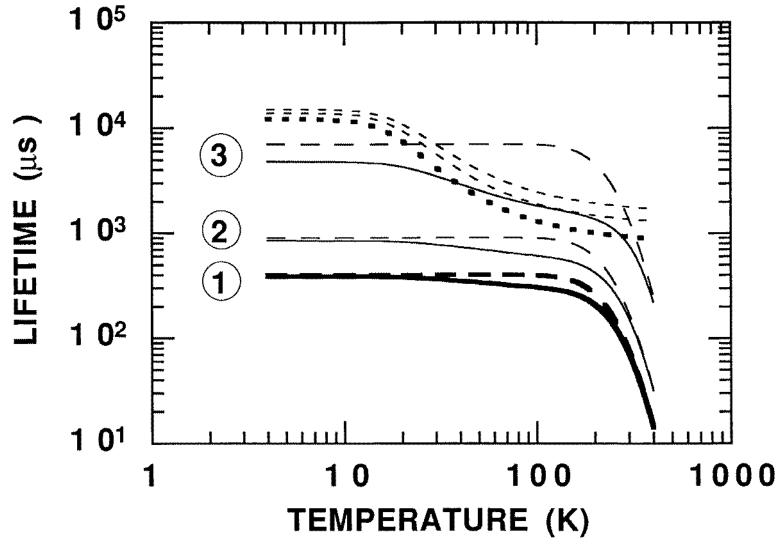

Figure 2. Temperature dependences of the transition times (equation (13)) for an energy of 1.86 eV: $\tau_{\rm rad}$ (short-dashed lines), $\tau_{\rm nr}$ (long-dashed lines) and τ (continuous line). Here we have used the same set of parameters as given in table 1 except for: case (1), thick lines: $\tau_{\rm sing}^{(0)} = 150$ μs, $\tau_{\rm nr}^{(0)} = 900$ μs; case (2), thin lines: $\tau_{\rm sing}^{(0)} = 100$ μs, $\tau_{\rm nr}^{(0)} = 400$ μs; and case (3), thin lines: $\tau_{\rm sing}^{(0)} = 200$ μs, $\tau_{\rm nr}^{(0)} = 7000$ μs.

2.4. The case of isolated Si nano-crystals

Let us consider the case in which no hopping between n.n. Si nano-crystals occurs in the system. This limiting situation may well describe porous Si samples in which Si nano-crystals are efficiently passivated and surrounded by thick surface oxide layers. This case represents an ensemble of isolated QDs, each characterized by its own size d and transition energy E. To obtain the luminescence spectrum of the whole ensemble as a function of time, for different observation energies and temperatures, the rate equation describing the time evolution of the density $N(t)$ for a single carrier at a given Si nano-crystal (site) is solved. Such a rate equation reads

$$\frac{\mathrm{d}N(t)}{\mathrm{d}t} = -\frac{N}{\tau_{\rm rad}} - \frac{N}{\tau_{\rm nr}} \tag{12}$$

and the exact solution is

$$N(t) = N(0)\exp(-t/\tau) \qquad \text{with } \frac{1}{\tau} = \frac{1}{\tau_{\rm rad}} + \frac{1}{\tau_{\rm nr}}. \tag{13}$$

Typical behaviours of the different times entering in equation (13) as a function of temperature, for fixed energy E, are shown in figure 2.

The luminescence $L(t)$ from a single Si nano-crystal is just $L(t) = N(t)/\tau_{\rm rad}$, i.e.

$$L(t) = L(0)\ \exp(-t/\tau) \tag{14}$$

yielding simple exponential decay, i.e. $\beta = 1$ (compare equation (1)). As pointed out in [8], the luminescence decay time is essentially determined by non-radiative recombinations at room temperature. According to equation (13) and figure 2, non-radiative recombinations play a major role also at low temperatures when the radiative lifetime, dominated by

the triplet recombination lifetime, becomes very large. In the intermediate-temperature range, when the quantum efficiency also increases, the singlet lifetime may dominate the recombination lifetime, if it becomes sufficiently small and thermal quenching of the phonon population takes place, decreasing the cross-section for capture to the non-radiative recombination centres. This is case 3 in figure 2. At sufficiently high temperatures, non-radiative recombinations dominate again.

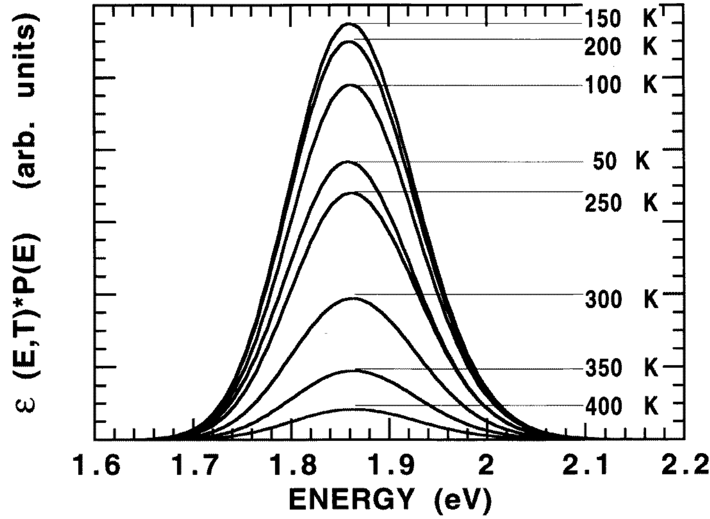

Figure 3. Quantum efficiencies of an ensemble of isolated quantum dots: $\epsilon(E,T)P(E)$ versus E for various temperatures given on the curves in K. The temperature dependence of the Si band-gap has been neglected. Note that only relative variations of the quantum efficiency as a function of temperature are relevant, and no appreciable energy shifts in the distributions are observed when temperature is changed.

The total radiated intensity

$$I(E,T) = \int_0^\infty \mathrm{d}t \; L(t) = N(0)\tau/\tau_{\mathrm{rad}}$$

is related to the corresponding quantum efficiency, $\epsilon(E,T)$ defined as

$$\epsilon(E,T) \equiv \frac{I(E,T)}{N(0)} = \frac{\tau_{\mathrm{nr}}}{\tau_{\mathrm{nr}} + \tau_{\mathrm{rad}}}. \tag{15}$$

For illustration, the quantity $\epsilon(E,T)P(E)$, representing the quantum efficiency of the ensemble of QDs described by equation (2) for an energy E, is plotted for several temperatures versus energy in figure 3. The total quantum efficiency of the ensemble, $\epsilon(T)$, is just the sum of equation (15) over the total number of Si nano-crystals in the system, i.e. $\epsilon(T) = \sum_E P(E)\epsilon(E,T)$. This quantity is shown in figure 4. At high temperatures, we find an exponential behaviour $\epsilon(T) \sim \exp(-T/T_0)$, where $T_0 \cong 59$ K (see cases (1) and (2) in figure 4), in good agreement with recent experimental results (see, e.g., [32]). The values $\hbar\omega_{ph}/k_B = 800$ K and $p = 25$ (see section 2.2) were chosen such that $\epsilon(T)$ displays a maximum in the range $100 < T < 200$ K and a value of about 10% at room temperature, as is experimentally observed [8].

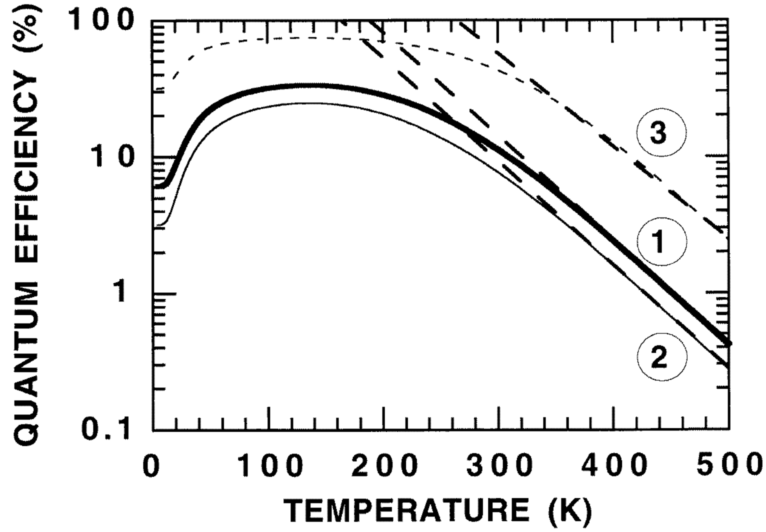

Figure 4. Total quantum efficiencies of the ensemble of quantum dots, $\epsilon(T)$, versus temperature. Here we have used the same set of parameters as given in table 1 except for: case (1), thick line: $\tau_{\text{sing}}^{(0)} = 150\ \mu$s, $\tau_{\text{nr}}^{(0)} = 900\ \mu$s; case (2), thin line: $\tau_{\text{sing}}^{(0)} = 100\ \mu$s, $\tau_{\text{nr}}^{(0)} = 400\ \mu$s; and case (3), thin dashed line: $\tau_{\text{sing}}^{(0)} = 200\ \mu$s, $\tau_{\text{nr}}^{(0)} = 7000\ \mu$s. The thick dashed lines represent the exponential behaviour $\epsilon(T) \sim \exp(-T/T_0)$, with $T_0 = 59$ K for case (1) and case (2) and $T_0 = 75$ K for case (3).

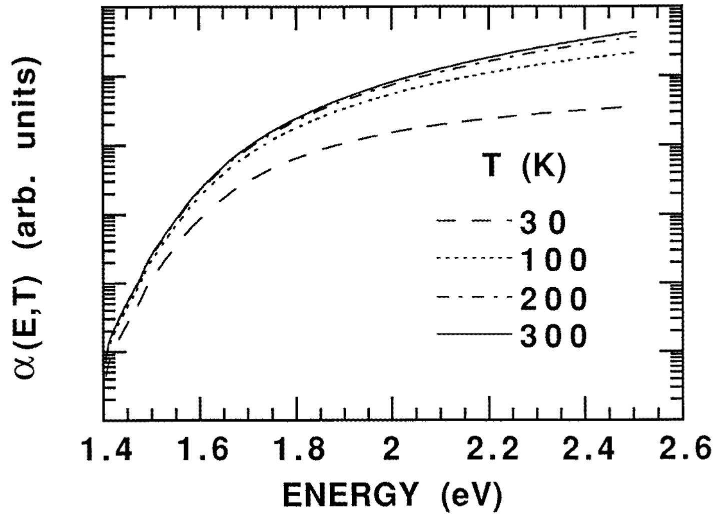

Figure 5. Absorption coefficients of the ensemble of isolated quantum dots, $\alpha(E, T)$, versus energy for the indicated temperatures, T.

Finally, the absorption coefficient $\alpha(E)$ of the ensemble can be obtained from the relation

$$\alpha(E, T) \simeq \frac{\text{constant}}{E}\ |M|^2 \rho(E) \qquad (16)$$

where $|M|$ is the dipole matrix element at the band-edge describing radiative transitions in the QD, and $\rho(E)$ is the total density of states. $|M|$ is related to the oscillator strength of the transition and hence to the radiative lifetime, i.e. $|M|^2 \sim \tau_{\text{rad}}^{-1}(E, T)$ [28]. Using the result obtained in section 2.1 for $\rho(E)$, equation (4), and expression (5) for τ_{rad}, we obtain the absorption coefficient of the ensemble as displayed, for various temperatures, in figure 5. Remarkably, this very simple model is able to reproduce the main features of the measured absorption coefficient [9], i.e. a quite sharp edge at about 1.6 eV and an increasing exponential shape at high energies with a slope which depends on the temperature. An exponential fit at high energies, $\alpha(E) \sim \exp(E/E_0)$, of the curves shown in the figure yields for the energy slopes: $E_0 = 0.55$ eV for $T = 30$ K, 0.34 eV for $T = 100$ K, 0.29 eV for $T = 200$ K and 0.28 eV for $T = 300$ K. The temperature dependence of $\alpha(E)$ is due to the τ_{rad}-term in equation (16). Similar exponential dependences of the absorption coefficient at large E have been repeatedly observed in porous Si [32, 33] at room temperature. Further measurements at different temperatures would be desirable.

2.5. Rules for the Monte Carlo simulations

In the case in which hopping of carriers between nearby Si nano-crystals takes place, the rate equation for $N(t)$, equation (12), is modified to

$$\frac{\mathrm{d}N_i(t)}{\mathrm{d}t} = -\frac{N_i}{\tau_{\text{rad}}} - \frac{N_i}{\tau_{\text{nr}}} - \sum_j P_{ij} N_i(t) + \sum_j P_{ji} N_j(t) \tag{17}$$

yielding a system of coupled differential equations for the different occupied sites i. For simplicity, we have omitted the index x, denoting the type of carrier, from equation (17). The third term in equation (17) represents the particles going out from site i (the loss term), while the last term represents the particles coming in to site i from the neighbour sites j (the feeding term). In one dimension, the number of nearest-neighbour sites $n = 2$, and because of structural disorder, in two dimensions $1 \leqslant n \leqslant 4$, and in three dimensions $1 \leqslant n \leqslant 6$. The system in equation (17) is conveniently solved by Monte Carlo (MC) simulations when the total number of effectively coupled occupied sites i becomes large (see, e.g., [34]). In particular, certain constraints for the occurrence of recombination processes, such as the simultaneous presence of an electron and a hole at a given site, can be easily implemented with the MC method.

Before discussing the MC rules, we need to determine the unit of time, denoted as τ_0, which should be sufficiently small that faster transition events are well described. Once the transition times τ have all been determined in the system, one can take $\tau_0 = \tau_{\text{fast}}/n_t$, where τ_{fast} is the smallest transition time in the ensemble and $n_t > 1$. We have used $n_t = 10$ in our simulations. Notice that the time t becomes now a discrete variable, i.e. $t = n\tau_0$, where $n \geqslant 1$ denotes the nth MC step. The total elapsed time for each MC step is just τ_0.

We can now discuss the MC rules for the present model. Since we are interested only in the case of very low carrier density, i.e. different electron–hole pairs in the system do not see each other (no interaction effects or Auger recombinations), we study the time evolution (trajectory) of a *single* electron–hole pair (either as an exciton or as two independent particles), which is initially located ($t = 0$) at the centre of the lattice. Averages are then performed over many trajectories and different realizations of disorder.

During the nth MC step, a particle at site i may undergo one of the following four different processes:

(1) decaying radiatively (annihilating) with a probability $p_{\text{rad}} = \tau_0/\tau_{\text{rad}}$;
(2) decaying non-radiatively (annihilating) with a probability $p_{\text{nr}} = \tau_0/\tau_{\text{nr}}$;

(3) hopping to a n.n. site j with a probability $p_{ij} = \tau_0 P_{ij}$; or
(4) remaining at site i with a probability $p_{\rm sit} = 1 - p_{\rm rad} - p_{\rm nr} - \sum_j p_{ij}$.

In the case in which an electron and a hole are considered, a decay can only take place when both carriers are located at the same site.

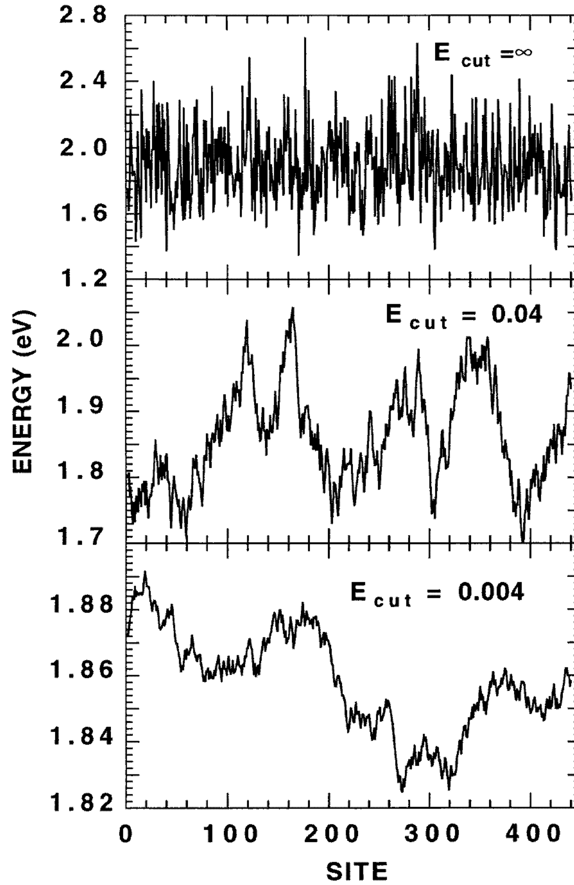

Figure 6. A snapshot of the energy landscape for diffusion in a one-dimensional lattice. The transition energy E is plotted versus position, for: $E_{\rm cut} = \infty$ (uncorrelated values, top panel); 0.04 eV (middle panel); and 0.004 eV (bottom panel). The mean energy value over the 29 791 sites is 1.86 eV for the three cases.

According to our definition of τ_0, all of the above probabilities are smaller than one as required. To decide which event will take place for a given particle at site i, we generate a random number r, uniformly distributed in the range $0 < r < 1$. Then, we evaluate the partial sums over the probabilities, i.e. $\sum_{k=1}^{m} p_k = S_m$, where the index $k = 1$ represents a radiative recombination event, $k = 2$ a non-radiative one, etc, and $m \geqslant 1$. The successful event is the one for which $S_m > r$ for the first time. For example, consider a 1D system and let $p_{\rm rad} = p_{\rm nr} = 0.2$ (equally likely radiative and non-radiative recombinations) and $p_{i(i-1)} = p_{i(i+1)} = 0.1$ (i.e. equal hopping rates to two n.n. sites). Then, if $r = 0.55$, the particle will undergo the fourth possibility, i.e. it will hop to the second n.n. site. If, however, $r > 0.6$, the particle will remain at its present site.

A single MC step is completed when the above-discussed procedure has been applied to each particle in the system (either the exciton, or the electron and hole), and the time t is increased by τ_0, $t = t + \tau_0$. At the nth MC step, corresponding to time $t = n\tau_0$, the luminescence of the system is simply obtained by counting the total number of radiative events during the nth MC step. Since we are also interested in the energy dependence of the luminescence, those radiative events originating at sites characterized by transition energies E' close to the observation energy E (i.e. $|E' - E| > \delta E$) are recorded separately. In our simulations we used $\delta E = 0.01$ eV.

We proceed with the numerical results obtained for one-dimensional lattices.

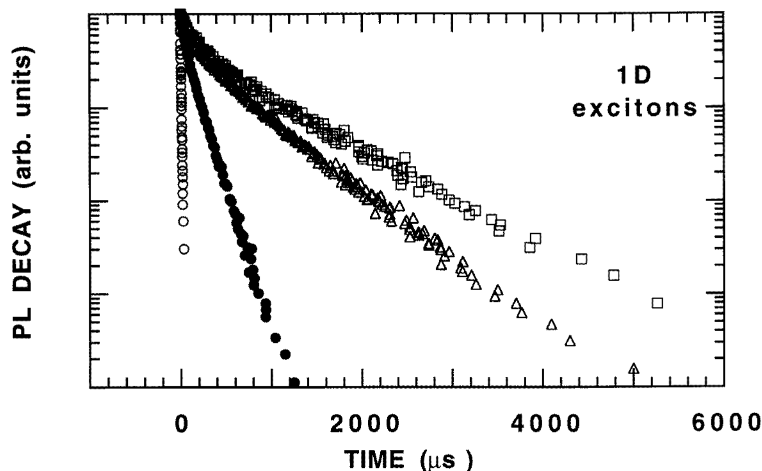

Figure 7. Monte Carlo simulation results for a one-dimensional system of excitons. Luminescence versus time for four different temperatures: $T = 20$ K (squares); 100 K (triangles); 300 K (full circles); and 500 K (empty circles).

3. Results for one-dimensional lattices

At very high porosities, porous Si is characterized by a filamentary structure having a quasi-one-dimensional character on small length scales [35]. Thus, we start our discussion about transport (diffusion) of carriers in porous Si on a simplified one-dimensional model. Preliminary results with the set of parameters named case (3) in figures 2 and 4 are reported in [19].

When the carriers are allowed to hop between n.n. sites of the linear lattice, the diffusive motion takes place in a highly irregular energy landscape. This feature of the model is illustrated in figure 6, where the local transition energies E are plotted as functions of position on the one-dimensional lattice. In the figure, three cases are considered for selected values of the parameter E_{cut} (see section 2.1). Although local variations in energy can be smoothed out when E_{cut} becomes sufficiently small, on large length scales appreciable variations of E will always occur (see figure 6). This has important consequences when considering hopping processes, because carriers must eventually overcome an effective large barrier to diffuse out of a region of local minimum energy. According to our definition of the transition rates in equation (10), thermally activated hopping against such large effective barriers will be strongly hindered at sufficiently low temperatures, even in the case of low

E_{cut}-values. The low-energy sites with low p_{rad} and high energy barriers ΔE_{ij} act as *temporary traps*. Excitons which relax to these sites are temporarily trapped into them and have to wait long times before being released.

To quantify the effect of disorder on diffusion we calculate the mean square displacement of the carrier as a function of time, $R^2 \equiv \langle r^2(t)\rangle - \langle \boldsymbol{r}(t)\rangle^2$, and investigate its temperature dependence. $\boldsymbol{r}(t)$ is the displacement with respect to the initial position, which is assumed to be the origin. To study the effect of the dynamics of carriers on the time dependence of $L(t)$, we have solved equation (17) for the values given in the table 1. Since in experiments all sites of the system are homogeneously excited at $t = 0$, including those with energy E close to the observation energy E_{obs}, initially, the electron–hole pair is placed at a site (the centre of the lattice) characterized by an energy $E \cong E_{\mathrm{obs}}$.

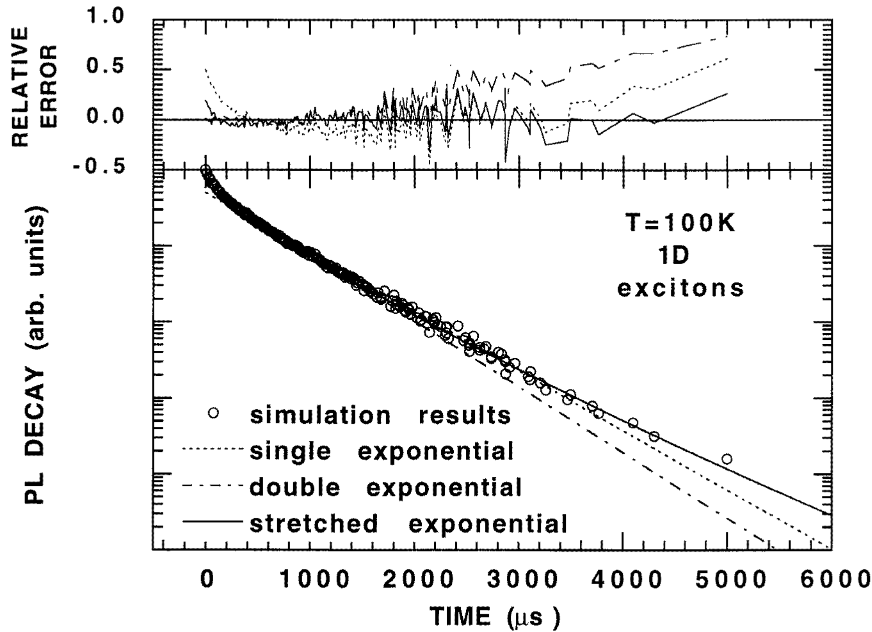

Figure 8. Fittings of the luminescence decay (circles) obtained from a Monte Carlo simulation for a one-dimensional system of excitons at $T = 100$ K. The following fitting functions and best-fit parameters have been used: stretched exponential function with $\tau = 345$ μs and $\beta = 0.815$ (full line); single-exponential decay with $\tau = 555$ μs (dotted line); double-exponential with $\tau_1 = 80$ μs and $\tau_2 = 503$ μs (dashed–dotted line). The top panel reports the relative errors, defined as the ratio of the difference of the simulation data (Y) minus the computed value (Y_{FIT}) times the simulation data, i.e. $[(Y - Y_{\mathrm{FIT}})/Y]$, for the three fitting functions.

In the case of excitons, the behaviour of the luminescence is shown in figure 7 for four different temperatures and observation energy $E_{\mathrm{obs}} = 1.86$ eV. Two features are evident: (i) the decay departs from the simple exponential decay obtained for isolated QDs (corresponding to $\tau_{\mathrm{hop}} = \infty$); and (ii) the time-scale of the decay is strongly temperature dependent. The last item is due to the thermal population of the singlet state (fast radiative recombination time) and to the onset of efficient non-radiative decay, especially at the highest temperature. The lineshape analysis shown in figure 8 provides evidence that a stretched exponential function is required to fit the decay. The single-exponential and the double-exponential functions are able to fit the decay only for a limited time range.

The stretched exponential decay reflects the fact that a time delay between recombination events at a given QD may occur when the exciton can diffuse out of the QD. Such time delay can persist on large time-scales since the exciton may either diffuse far away from the site at which the radiative event is expected, or may become temporarily *trapped* at a nearby site with a lower transition energy. When the observed radiative events are collected from sites with similar transition energies E, the random local environment around each of these sites leads to a distribution of recombination times, which are in general different to the single value $\tau_{\rm rad}(E, T)$ for that energy E. This *dispersion* of recombination times causes the stretched exponential behaviour observed in the model.

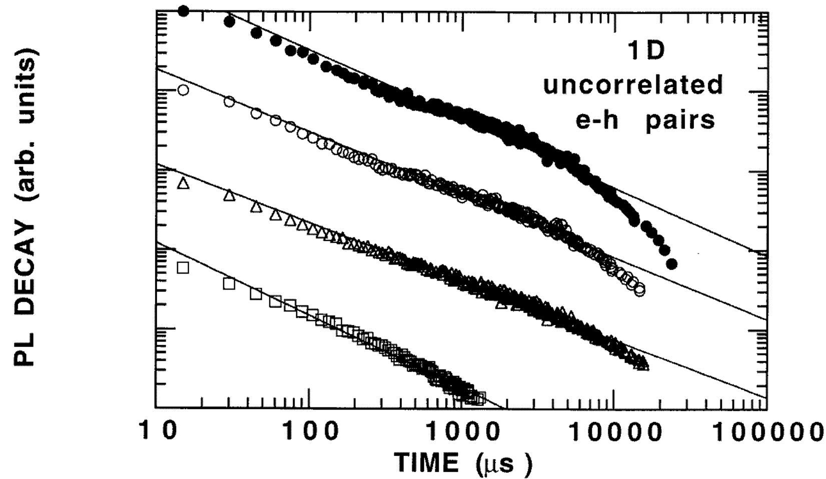

Figure 9. Monte Carlo simulation results for a one-dimensional system of uncorrelated electron and hole pairs. Luminescence versus time for four different temperatures: $T = 30$ K (dots); 50 K (circles); 100 K (triangles); and 300 K (squares). The lines are power-law fits to the decay with the following exponents: $\alpha = 0.86$ ($T = 30$ K); 0.79 ($T = 50$ K); 0.73 ($T = 100$ K); and 0.91 ($T = 300$ K). The curves are vertically shifted for clarity.

In the case of uncorrelated electron and hole motion, a quite different behaviour is observed (see figure 9). At high temperatures, and intermediate times, an approximate power-law decay of the form

$$L(t) \sim t^{-\alpha} \tag{18}$$

takes place. The range of times over which the power-law decay seems to occur grows as the temperature is raised. Here, the uncorrelated motion of the electron and hole leads to a dramatic slowing down of the luminescence decay, since the two carriers are no longer constrained to be all the time simultaneously at the same site. Similar lineshapes have been observed for amorphous hydrogenated silicon [36]. In this system, the luminescence is explained as due to geminate recombination between e–h pairs localized in band-tail states [37].

We have performed extensive MC simulations for different temperatures. In the case of excitons, the decay lineshapes are fitted by a stretched exponential function for all of the temperatures considered. A statistical weight of the simulation points has been used to obtain the best-fit function. The results of the fits are summarized in the upper panel of figure 10. Typical errors for τ of 10% and β of 0.02 are expected, due to statistical fluctuations and the goodness of the fits. The lifetime τ decreases significantly as the

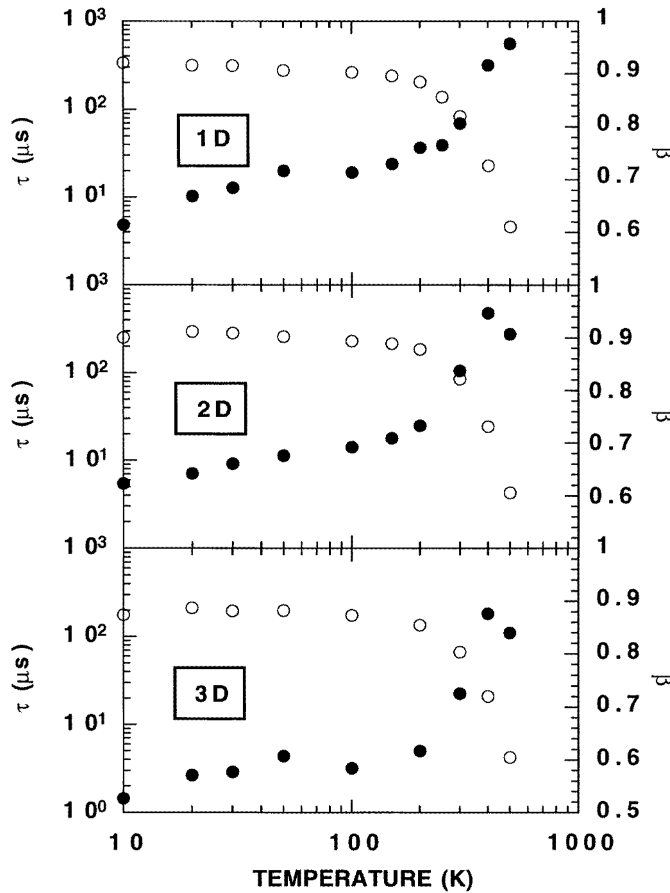

Figure 10. Temperature dependences of the luminescence recombination time τ (circles) and dispersion exponent β (full circles) obtained by a stretched exponential fit to the time decay of the luminescence, for an exciton population in one-dimensional (upper panel), two-dimensional (middle panel) and three-dimensional (lower panel) clusters.

temperature is raised, while the dispersion exponent β increases and tends to unity at high temperatures.

We have also calculated the quantum efficiency $\epsilon(E, T)$ as a function of E for a fixed temperature, displaying a maximum at around $E = 1.86$ eV and found that hopping of carriers does not sensitively affect $\epsilon(E, T)$. This is clear because $\epsilon(E, T)$ is essentially determined by the on-site recombination dynamics. Independently of the dispersive motion, all of the carriers recombine radiatively or non-radiatively after a sufficiently long time. The diffusion only influences the recombination dynamics by introducing long-lived recombinations.

In figure 11, we show the values of $R^2(t)$ for different temperatures. At low temperatures, an anomalous behaviour of the form $R^2(t) \sim t^{2/d_w}$ with $d_w \geqslant 2$, takes place (figure 12). These anomalies are due to the random distribution of hopping rates, which is known to yield values of $d_w > 2$ and dependent on temperature (see, e.g., [38, 39, 40]). At low temperatures, however, the time dependence of $R^2(t)$ departs from a power law and

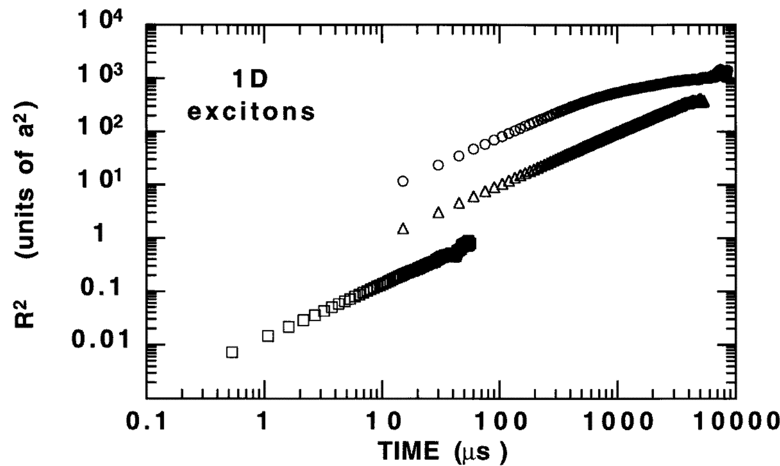

Figure 11. Mean square displacements $R^2(t)$ of excitons in one dimension for three different temperatures: $T = 20$ K (circles); 100 K (triangles); and 500 K (squares). Here, a is the lattice constant. The straight lines have slopes corresponding to $d_w = 2$ ($T = 500$ K), and $d_w = 2.07$ ($T = 100$ K). At $T = 20$ K, strong deviations from a straight line occur, indicating that a power-law *ansatz* for $R^2(t)$ is no longer appropriate. The curves are vertically shifted for clarity by factors: $f = 100$ for $T = 20$ K; and $f = 10$ for $T = 100$ K.

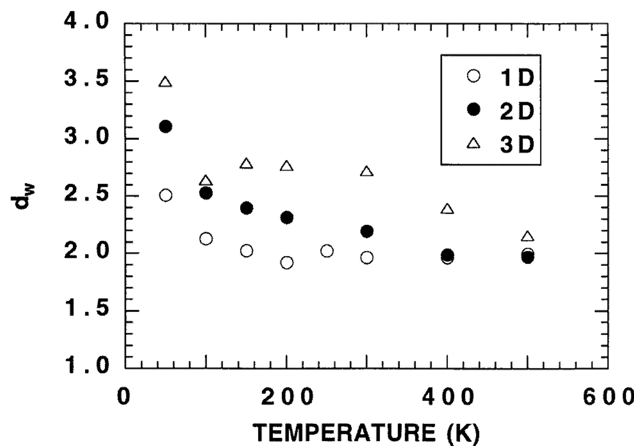

Figure 12. Anomalous diffusion exponents d_w obtained by a power-law fit to the mean square displacements $R^2(t)$ of excitons in one-dimensional (circles), two-dimensional (full circles) and three-dimensional (triangles) clusters.

logarithmic time dependences occur (see also [40]).

At sufficiently low temperatures, indeed, the present model is expected to display transport behaviour similar to diffusion in the presence of random fields (the Sinai model); see [41] and [42]. To show this, we have drawn in figure 13 a small section of a typical energy landscape versus position. The arrows represent the local *fields* felt by the carrier which are proportional to the energy difference ΔE_{ij} between the two n.n. sites i and j. Due to the assumed random distribution of nano-crystal sizes in the system, the local fields

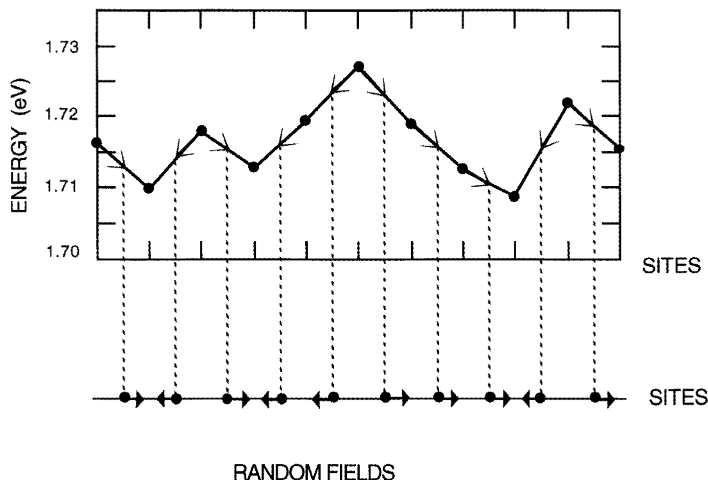

Figure 13. The energy landscape (transition energies E versus position) in one dimension. The arrows are drawn in direct correspondence with the local energy difference between nearby sites. The resulting one-dimensional chain (lower panel) is equivalent to the Sinai model, in which uncorrelated random fields are present at each site of the lattice.

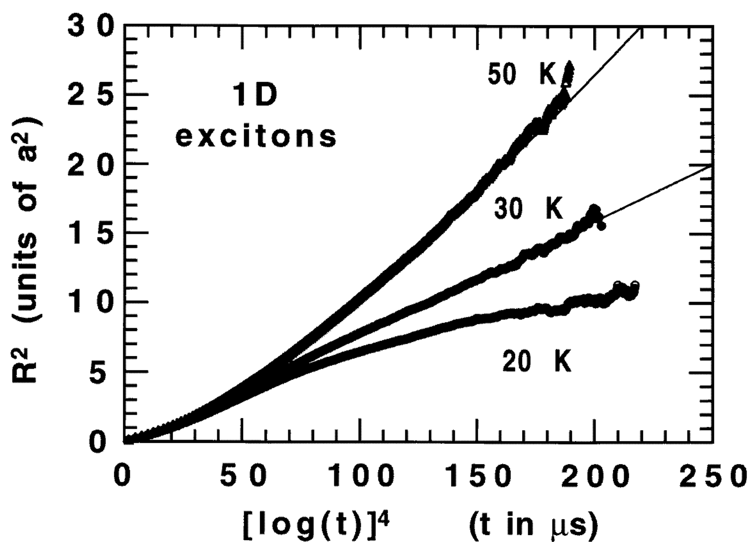

Figure 14. Mean square displacements $R^2(t)$ of excitons in one dimension plotted versus $(\log t)^4$ for the temperatures: $T = 20$ K; 30 K; and 50 K. Here, a is the lattice constant. The straight line through the $T = 30$ K results represents the asymptotic $(\log t)^4$-behaviour. The line through the $T = 50$ K results shows the power-law t^{2/d_w}-behaviour, with $d_w = 2.5$.

are randomly oriented, similarly to in the Sinai model. Diffusion of carriers in the system is biased by these random fields and becomes ultra-anomalously slow. Of course, in the present model the energy barriers (and also the potential valleys) cannot grow indefinitely as in the Sinai case. However, when the temperature is sufficiently low, diffusion is strongly

hindered and the carriers can only explore small length scales since the effect of the random fields becomes dominant. In these circumstances, a logarithmic time dependence is expected

$$R^2(t) \sim (\log t)^4 \tag{19}$$

at long times. Results obtained for the case of excitons are plotted in figure 14. These suggest that for large times and low temperatures, our model displays logarithmic time dependencies of the form predicted by equation (19). To our knowledge, this is the first time that such logarithmic time dependencies of $R^2(t)$ have been predicted for a model aimed at describing a disordered system such as porous silicon. Actually, the value of the exponent describing the logarithmic time dependence turns out to depend slightly on temperature, and the value of four is observed only for $T \cong 30$ K. At lower T, R tends to extrapolate to a constant value because the carriers are annihilated (non-radiative annihilation events dominate) and the carriers can only explore a finite spatial extent asymptotically. A similar trend is also observed for electrons and holes in the case of uncorrelated electron–hole pairs.

4. Two- and three-dimensional models and results

The actual geometrical structure of porous silicon is not known accurately. For many purposes, however, one may hope to capture the essential features of such complex structures by modelling them with simple, yet non-trivial, percolation-like clusters [43]. The clusters are generated by using a modified version of the well-known growth algorithm employed for percolation clusters (see, e.g., [43]), which is adapted here to our present purposes.

For simplicity we consider a square lattice in two dimensions, and a simple cubic one in three dimensions. The linear size of the lattice is denoted by ℓ. The growing process starts at the seed, which is located at the centre of the otherwise empty lattice. The growth proceeds according to the following rules. A nearest-neighbour site j of the seed can be occupied with probability p_n, with the index n indicating the number of occupied sites nearest to the growing site j. Initially, $n = 1$. If the site j is not occupied, i.e. if it does not become part of the cluster, it is blocked and cannot be occupied later. The process continues from the last occupied sites and now values $n > 1$ may occur.

For standard percolation clusters, one takes $p_n = p$ independently of n. When $p < p_{\rm crit}$, $p_{\rm crit} \cong 0.593$ (two dimensions), and $p_{\rm crit} \cong 0.312$ (three dimensions), only finite clusters can grow, while infinite clusters develop when $p > p_{\rm crit}$. When $p = p_{\rm crit}$, large percolation clusters may grow which are fractal (with fractal dimension $d_{\rm f} \cong 1.896$ in two dimensions, and $d_{\rm f} \cong 2.5$ in three dimensions) on large length scales. Finite clusters and the infinite cluster above $p_{\rm crit}$ are also fractal (with the same fractal dimension $d_{\rm f}$) for length scales smaller than the correlation length. The latter diverges at $p = p_{\rm crit}$.

In our model, we take $p_1 > p_2$ and $p_n = 0$ when $n > 2$. In the following, we consider for illustration the cases $p_1 = 0.65$ and $p_2 = 0.15$ in two dimensions, and $p_1 = 0.45$ and $p_2 = 0.17$ in three dimensions. (A detailed discussion of the effects of varying the growth parameters p_1 and p_2 on the luminescence exceeds the scope of the present work.)

We notice that when $p_1 \to 1$, and $p_2 \to 0$, the clusters tend to grow linearly, while for relatively large p_2, compact clusters can be grown. By varying both p_1 and p_2, a variety of structures can be obtained which are suitable for our present purposes. A measure of the *porosity* of the cluster is simply given by the ratio between empty sites and occupied sites. Typical examples are shown in figure 15 for three-dimensional clusters, and in [20] for two-dimensional clusters. The clusters are uniform on large length scales, but still display spatial fluctuations on small length scales, similar to the infinite cluster above $p_{\rm crit}$ [20]. Thus, the intrinsic fractal character of percolation is common to the clusters shown

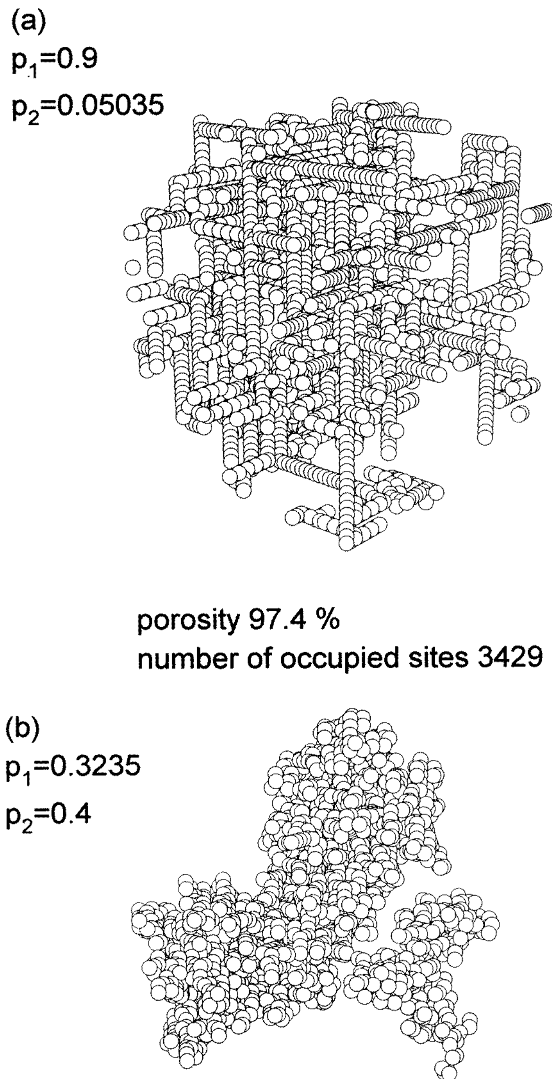

Figure 15. Percolation-like clusters grown on a simple cubic lattice representing porous silicon of the same 97.4% porosity but different growth probabilities: (a) $p_1 = 0.9$, $p_2 = 0.050\,35$; (b) $p_1 = 0.3235$, $p_2 = 0.4$.

in figure 15 too. It is possible to construct highly constrained and filamentary clusters (like that in figure 15(a)) or more compact clusters (like that in figure 15(b)).

We have studied the dynamical behaviour of carriers on these clusters, following the same MC rules as described above. The question now is how the extra degrees of freedom in space, resulting from the two- or three-dimensional topology of the clusters, modify the time decay of $L(t)$. Preliminary results for two-dimensional systems have been reported in [44]. Results for three-dimensional systems are reported in figure 16 for the luminescence decay [20]. For excitons and uncorrelated electron–hole pairs, the lineshape is a stretched exponential and a power law, respectively. Hence the decay lineshape is not modified by the

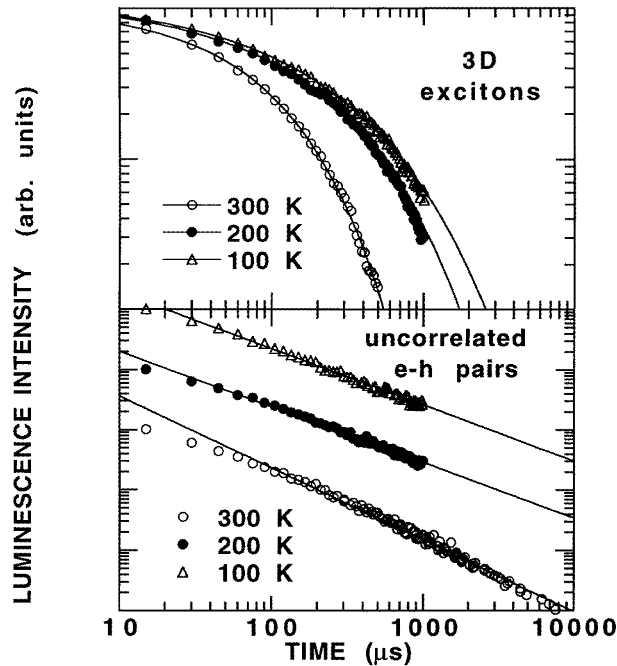

Figure 16. The luminescence decay of a three-dimensional system of excitons (upper panel) and of uncorrelated electron–hole pairs (lower panel) for three different temperatures: $T = 300$ K (circles); 200 K (full circles); and 100 K (triangles). The lines are fits to the luminescence decays. Stretched exponentials have been used for the exciton case with the following parameters: $\tau = 175$ μs and $\beta = 0.58$ ($T = 100$ K); $\tau = 135$ μs and $\beta = 0.62$ ($T = 200$ K); and $\tau = 66$ μs and $\beta = 0.73$ ($T = 300$ K). Power laws, $t^{-\alpha}$, have been used for the uncorrelated electron–hole pairs with the following parameters: $\alpha = 0.96$ ($T = 100$ K); $\alpha = 1.10$ ($T = 200$ K); and $\alpha = 1.28$ ($T = 300$ K). In this case, the curves are vertically shifted for clarity.

increased dimensionality. Results of stretched exponential fits to the luminescence decay in two or three dimensions, for the exciton model, are reported in figure 10 as a function of temperature.

The three-dimensional topology has important consequences for the decay of the luminescence. The τ- and β-values are lower, indicating that the role of hopping processes in three dimensions is more important than in lower dimensions. While the one-dimensional model (and also the two-dimensional one) predicts values of β close to unity already at room temperature, in three dimensions, in contrast, the theoretical values are consistent with the experimental results for β, which typically saturate at values of $\beta \cong 0.7$–0.8 [18, 19]. Thus, values of $\beta < 1$ at high temperatures, and intermediate porosities, can be explained by our model as the result of the interplay between a complex conducting matrix (representing the topology of porous Si), and an additional local disorder due to the distribution of nano-crystal sizes in the system.

A comparison of the temperature dependence of τ and β for two different sets of parameters (but for the same growth parameters p_1, p_2 as mentioned above) is reported in figure 17. The effect of varying τ_{nr} is evident in β: the larger the τ_{nr} the lower is β. The role of temporary traps, which tend to reduce β and are effective at low temperatures, is enhanced when τ_{nr} is increased due to a relative increase of the role of exciton diffusion

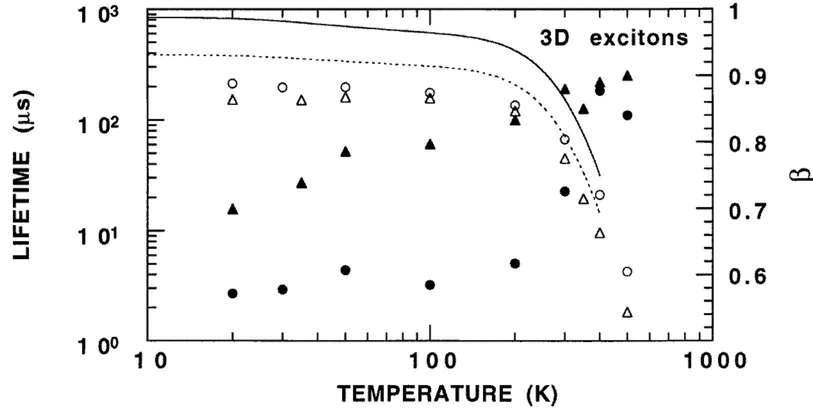

Figure 17. Temperature dependences of the luminescence recombination times τ (empty symbols) and dispersion exponents β (filled symbols) for excitons in three-dimensional clusters and for two different sets of parameters. Circles correspond to case (1) of figure 2 and to the standard set of parameters reported in table 1. Triangles correspond to case (2) of figure 2 and hopping time $\tau_{\rm hop} = 100\ \mu$s. The lines are the lifetimes calculated using equation (13) in the case of isolated quantum dots, i.e. without hopping, for case (1) (full line) and case (2) (dotted line).

$(\sim \tau_{\rm nr}/\tau_{\rm hop})$.

The dynamics of carriers is influenced by the parameters p_1 and p_2 used to construct the clusters. The more the cluster is filamentary (see, e.g., case (a) in figure 15), the more the excitons are constrained to move along one direction, and the larger are τ and β. Then, the dynamical behaviour of carriers should have essentially a one-dimensional character, at least for sufficiently low temperatures where transport along the structure is strongly hindered. Thus, we expect to observe, in this regime, the same logarithmic time dependence of $R^2(t)$ as in the one-dimensional model, equation (19), at short times.

For arbitrary porosities and not too low temperatures, we find anomalous behaviour of $R^2(t) \sim t^{2/d_w}$, at intermediate times (figure 18). Here, $d_w > 2$ and increases as the temperature decreases, more than in the one-dimensional case (figure 12), and is typical of diffusion in the presence of a distribution of hopping rates (see, e.g., [38, 39, 40]). One should note that anomalies in $R^2(t)$ are typical of diffusion on fractals too. In these systems, however, the anomalies have a purely geometrical origin and are due to the structural constraints of the fractal, i.e. dangling ends and loops on all length scales, which slow down the diffusion process on all time-scales. On fractals, however, the diffusion exponent d_w is temperature-independent [43], while here d_w turns out to depend strongly on temperature (see figure 12). The intrinsic fractal behaviour of $R^2(t)$ can only be observed for distances $R^2(t) < \xi$, where ξ is the correlation length within which the clusters are fractal, and at high temperatures such that the effect of the energy barriers can be neglected. Under these circumstances one can expect to observe a temperature-independent exponent $d_w > 2$. In three dimensions, $d_w \cong 3.8$ for percolation clusters at criticality (see, e.g., [43]). Since our clusters are compact already at intermediate length scales, the true fractal behaviour discussed above cannot actually be reached. We conclude that the anomalies that we found are due to the distribution of energy barriers, which are enhanced by a strong local geometrical disorder.

The situation is different at low temperatures, where the carriers can only explore

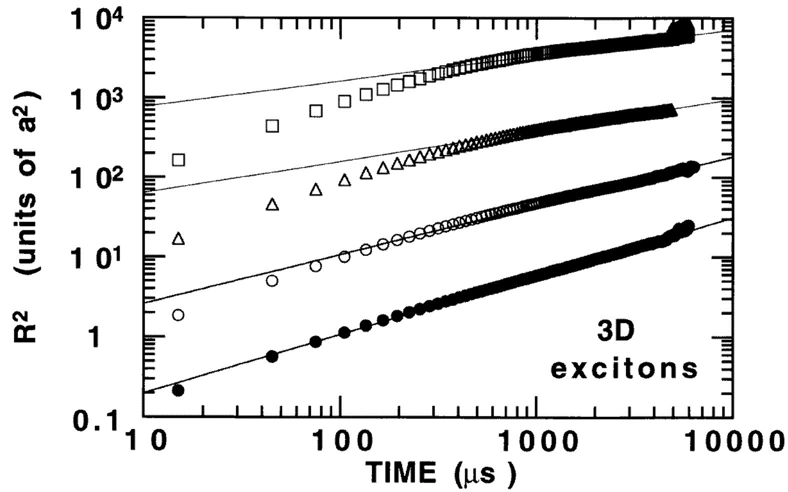

Figure 18. Mean square displacements $R^2(t)$ of excitons in three-dimensional clusters for four different temperatures: $T = 20$ K (squares); $T = 30$ K (triangles); $T = 50$ K (circles); and $T = 100$ K (full circles). Here, a is the lattice constant. The curves are vertically shifted for clarity by factors: $f = 1000$ for $T = 20$ K; $f = 100$ for $T = 30$ K; and $f = 10$ for $T = 50$ K. The lines are power-law fits with effective anomalous exponents: $d_w = 2.62$ ($T = 100$ K); 3.5 ($T = 50$ K); 5.16 ($T = 30$ K); and 6.4 ($T = 20$ K). Note, however, the bending of the data at low temperatures and long times, indicating that a power-law fit to data is no longer appropriate.

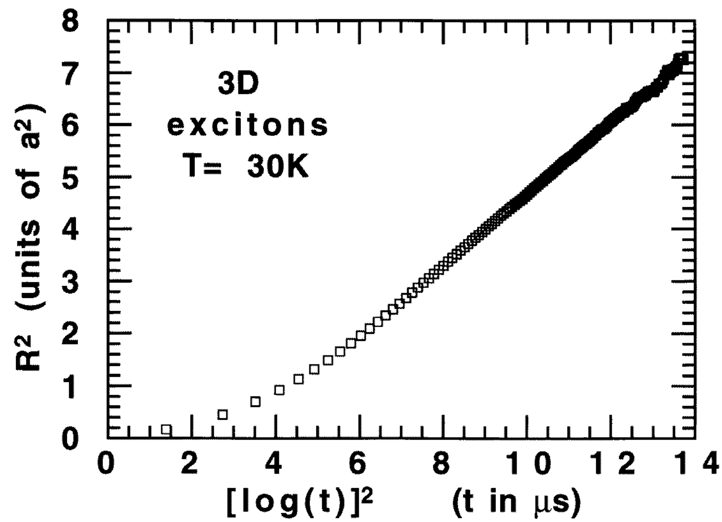

Figure 19. The mean square displacement $R^2(t)$ of excitons in three-dimensional clusters for the temperature $T = 30$ K, plotted as a function of $(\log t)^2$. Here, a is the lattice constant. Note the linear increase at long times.

their local environment, and effects due to both the distribution of energy barriers and the underlying fractal structure of the clusters play a role. Indeed, at sufficiently low T,

we have observed again a logarithmic time dependence of $R^2(t)$. In three dimensions, we have found clear evidence for the behaviour

$$R^2 \sim (\log t)^2 \tag{20}$$

at long times (figure 19), in contrast to the fourth-power result valid for the Sinai model in one dimension. This new behaviour represented by equation (20) has been predicted for the case of biased diffusion on random fractals in two dimensions [42]. Such a biased diffusion problem is equivalent to the presence of energy barriers at small length scales in our model, as discussed for the one-dimensional case (figure 13). As we can see from the present results, a behaviour $R^2 \sim (\log t)^2$ can be expected also in three dimensions. We should note that logarithmic dependences have been already reported in the literature for exciton dynamics in amorphous systems for infinite-range-hopping models [40], but a direct relation with the present results, in which only jumps between nearest-neighbour available sites are allowed, is not straightforward.

5. Discussion

According to the present model, the photoluminescence decay, $L(t)$, is determined, in the case of excitons, by the rates of recombination and escape from the isolated QD. In the case of uncorrelated electron–hole pairs, $L(t)$ is determined by the diffusion of the electron and the hole, because both need to be on the same QD to recombine radiatively.

In the case of excitons, the disordered environments of the QDs, from which the luminescence is observed, cause a distribution of waiting times for hopping and/or release times for activated emission from the temporary traps, and the luminescence displays a stretched exponential decay. In the case of uncorrelated electron–hole pairs, the main role is played by the encounter probability of the electron and hole, i.e. the probability that both carriers meet on the same site. In this regime, the time dependence of the recombination rate becomes a power law [23], which is then reflected in the luminescence decay.

For all spatial dimensions D, the increase in β is almost linear for $10 < T < 60$ K, has a plateau for $60 < T \leqslant 200$ K and then increases rapidly to 1 at higher temperatures. This behaviour corresponds to the following three typical regimes: a first one in which the temporary traps play a role (low temperatures); a second one in which hopping dominates and diffusion is restricted only by the porous Si network geometry (intermediate temperatures); and a third one, in which the rapid on-site non-radiative recombinations are most effective and dominant (high temperatures).

Whereas there is general agreement among different experimentalists that τ strongly depends on temperature [7, 8, 18], the situation is less clear regarding the exponent β. While some authors report values of $\beta \cong 0.8$–0.9, independent of the temperature [15, 16], others found temperature-dependent values [17, 18, 19]. In this case, the β-values follow similar temperature and energy dependences in the range 0.4–0.8. By varying the parameters in our model, we are able to describe both situations. Temperature-dependent β-values are shown in figure 17. Temperature-independent values can be obtained when $\tau_{\mathrm{hop}} < \tau_{\mathrm{nr}}$ and τ_{sing}, since in this case the activation term in equation (10), which is mainly responsible for the temperature dependence of β, does not influence the diffusion of carriers, being only restricted by the geometrical constraints of the porous Si network.

By going from an interconnected array of QDs to an ensemble of isolated QDs our model predicts that the lifetime τ and the dispersion exponent β increase, with β taking values near 1. This has indeed been observed in several experiments. For example, the data presented in [45], and reanalysed using stretched exponential functions, show that τ

and β increase after dry oxidation of porous Si. It is well known that the interconnected array of QDs typical of porous Si is transformed after dry oxidation into a dispersion of nano-crystals immersed in a SiO_x matrix; on further increasing the oxidation a porous glass is formed [6].

Our simulations show that hopping of excitons is responsible for the stretched exponential decay observed in porous Si. This rules out other explanations which are based on analogies with hydrogenated amorphous Si (a-Si:H); see, e.g., [46]. In fact we demonstrated that PL decay lineshapes, strongly resembling those measured for a-Si:H, are found for uncorrelated e–h pairs. This behaviour can possibly explain the lack of room temperature luminescence in a-Si:H. In fact, it is possible that the fast-diffusing species in the pair is rapidly trapped into non-radiative recombination centres when the thermal energy is sufficiently large to promote the particle to extended states [47].

Table 2. 300 K simulation results for a 3D clusters of 65% porosity as a function of the time parameters: $\tau_{nr}^{(0)}$ and τ_{hop}. The other parameters are given in table 1.

$\tau_{nr}^{(0)}$ (μs)	τ_{hop} (μs)	τ (μs)	β	QE (%)
900	150	72	0.77	12
800	300	84	0.87	10
800	100	59	0.72	10
500	150	51	0.84	7

Annealing treatments induce a quenching of the room temperature luminescence with a decrease in the values of τ and β [14]. Within our model, this is simulated by diminishing $\tau_{nr}^{(0)}$ and τ_{hop} yielding lower values of τ, β and quantum efficiency (see table 2). The separate effects of varying $\tau_{nr}^{(0)}$ and τ_{hop} are the following.

(a) Reducing the non-radiative lifetime yields an increase of β and a decrease of τ. The reason for this is that the re-population of the target QDs, those from which the luminescence decay is recorded, is reduced by the competitive non-radiative recombination channels. Fewer excitons reach the target QD at long times because a large part recombine non-radiatively as they diffuse through the system. The target QD effectively behaves as being more isolated (increase of β). Then, τ is reduced due to the competing on-site non-radiative recombinations, and consequently the quantum efficiency is also reduced.

(b) Reducing τ_{hop} yields a reduction of τ and β. In fact, for higher hopping probabilities, the target QDs are emptied faster due to the competing loss of excitons caused by hopping (reducing τ), while at long times more excitons reach the target QD giving rise to long-lived recombinations (reducing β). In this case, no variations in the quantum efficiency are expected.

Hence to obtain the trends measured during the annealing experiments both the lifetimes, $\tau_{nr}^{(0)}$ and τ_{hop}, should be reduced.

Let us compare our simulations with other models. The non-exponential decay of $L(t)$ has been explained as due to a distribution of τ_{rad}-values arising from a shape distribution of quantum dots with the same emission energy [7, 48]. Within this assumption, however, it is difficult to explain the temperature dependence of β already discussed. It has also been proposed that the non-exponential behaviour of $L(t)$ is a consequence of a distribution of non-radiative decay rates [49, 50]. This fact is not considered in our model, and a refined version of it should certainly contain such a dependence. However, we want to

emphasize here that it is the dispersive motion of excitons which is mostly responsible for the non-exponential decay of $L(t)$. The radiative and non-radiative lifetime distributions could indeed concur to produce a similar effect on $L(t)$, but in isolated and well passivated quantum dots it is reasonable to expect essentially a simple exponential decay of $L(t)$. Such a behaviour has indeed been observed for some porous Si samples [51] and for Ge nano-crystals [52].

The strong temperature dependence of the effective anomalous diffusion exponent d_w, and the logarithmic time dependencies of $R^2(t)$ at lower temperatures, have important consequences for the ac conductivity, which is expected to display a strong frequency dependence at low temperatures. This observation is supported by recent experimental results on the ac conductivity of porous Si [53]. In contrast, at higher temperatures, diffusion becomes normal, $R^2(t) \sim t$, i.e. $d_w \to 2$, and the dispersion frequency range shrinks considerably. It should be emphasized that a model for the structure of porous Si has been suggested recently [53] in which the porous Si network is assumed to be the infinite percolation cluster above criticality. From our present results, however, one can see that such a model is far too simple to describe porous Si samples of different porosities, and a more elaborate model is required. In addition, theoretical results for the ac conductivity discussed so far [53] have been obtained using mean-field approximations, and the new intrinsic behaviour suggested here for diffusion of carriers in porous Si at low temperatures cannot be obtained.

6. Conclusion

The theoretical results obtained in this paper have for the moment a semi-quantitative character. A quantitative comparison between the present results and the available experimental data can be made possible when the parameters entering the model may be estimated independently and more accurately. Also, the precise relations between the nano-crystal structure and dynamical properties are so far unknown. We have tried to make up for this lack by making *ad hoc*, yet standard assumptions which seem to describe the physics of porous Si rather well. In addition, the actual values of the parameters are so strongly sample dependent and influenced by various treatments (ageing, oxidation, storage, excitation conditions, etc) that quantitative predictions valid in general are not possible. However, several experimentally measured trends in the photoluminescence life-times, dispersion exponents and quantum efficiencies of the luminescence are correctly explained in the framework of the present calculations by choosing the free parameters of the model appropriately. This gives strong support for the validity of the present model for describing the recombination dynamics in porous Si.

Finally, by assuming different forms for the various quantities reported in section 2, other systems can be described as well by the present model—for example, nanometre-sized Si crystallites [54], and CdSSe quantum dots [55]. All of these systems show a stretched exponential decay of the luminescence.

References

[1] Canham L T 1990 *Appl. Phys. Lett.* **57** 1046
[2] Feng Zhe Chuan and Tsu R (ed) 1995 *Porous Silicon* (New York: World Scientific)
Vial J-C and Derrien J (ed) 1995 *Porous Silicon Science and Technology* (Les Ulis: Les Editions de Physique)
[3] Benshael D C, Canham L T and Ossicini S (ed) 1993 *Optical Properties of Low Dimensional Silicon Structures (NATO ASI Series, vol 244)* (Dordrecht: Kluwer Academic)

[4] 1993 Light emission from silicon *J. Lumin.* **57** special issue
1995 Porous silicon and related materials *Thin Solid Films* **255** special issue
[5] Smith R L and Collins S D 1992 *J. Appl. Phys.* **71** R1
[6] Canham L T 1993 *Optical Properties of Low Dimensional Silicon Structures (NATO ASI Series, vol 244)* ed D C Benshael, L T Canham and S Ossicini (Dordrecht: Kluwer Academic) p 81
[7] Calcott P D J, Nash K J, Canham L T, Kane M J and Brumhead D 1993 *J. Phys.: Condens. Matter* **5** L91; 1993 *J. Lumin.* **57** 257
[8] Vial J C, Bsiesy A, Fishman G, Gaspard F, Herino R, Ligeon M, Muller F, Romestain R and Macfarlane R M 1993 *Mater. Res. Soc. Symp. Proc.* **283** 241
[9] Koch F 1993 *Mater. Res. Soc. Symp. Proc* **298** 319
Koch F, Petrova-Koch V and Muschik T 1993 *J. Lumin.* **57** 271
Koch F and Petrova-Koch V 1995 The surface state mechanism for light emission from porous silicon *Porous Silicon* ed Zhe Chuan Feng and R Tsu (New York: World Scientific) p 133
[10] Prokes S M, Glembocki O J, Bermudex V N, Kapla R, Friedersdorf L E and Searson P C 1992 *Phys. Rev.* B **45** 13 788
[11] Brandt M S, Fuchs H D, Stutzmann M, Weber J and Cardona M 1992 *Solid State Commun.* **81** 307
[12] Lavine J M, Sawan S P, Shieh Y T and Bellezza A J 1993 *Appl. Phys. Lett.* **62** 1099
[13] Chen X, Henderson B and O'Donnel K P 1992 *Appl. Phys. Lett.* **60** 2672
[14] Ookubo N, Ono H, Ochiai Y, Mochizuki Y and Matsui S 1992 *Appl. Phys. Lett.* **61** 940
[15] Kondo M 1993 *J. Non-Cryst. Solids* **164–166** 941
[16] Kanemitsu Y 1993 *Phys. Rev.* B **48** 12 357
[17] Ookubo N, Hamada N and Sawada S 1994 *Solid State Commun.* **92** 369
Ookubo N and Sawada S 1995 *Phys. Rev.* B **51** 17 526
[18] Pavesi L and Ceschini M 1993 *Phys. Rev.* B **48** 17 625
[19] Pavesi L, Ceschini M and Roman H E 1995 *Thin Solid Films* **255** 67
[20] Pavesi L and Roman H E 1995 *Mater. Res. Soc. Symp. Proc.* **358**
[21] Pfister G and Scher H 1978 *Adv. Phys.* **27** 747
[22] Klafter J and Shlesinger M F 1986 *Proc. Natl Acad. Sci. USA* **83** 848
[23] Scher H, Shlesinger M F and Bendler J T 1991 *Phys. Today* **44** 26
[24] Dumas P *et al* 1993 *Europhys. Lett.* **23** 197
[25] A generic quantity X, representing for instance the particle size d, is labelled with an index i, X_i, to indicate its actual local value at the ith site.
[26] Delerue C, Lannoo M and Allan G 1993 *J. Lumin.* **57** 249
[27] Yoffe A D 1993 *Adv. Phys.* **42** 173
[28] Hybertsen M S 1994 *Phys. Rev. Lett.* **75** 1514
[29] Fishman G, Romestain R and Vial J C 1993 *J. Lumin.* **57** 235
[30] Ridley B K 1978 *J. Phys. C: Solid State Phys.* **11** 2323
[31] Dorigoni L, Bisi O, Bernardini F and Ossicini S 1996 *Phys. Rev.* B **53** 4557
[32] Rosenbauer M, Stutzmann M, Fuchs H D, Finkbeiner S and Weber J 1993 *J. Lumin.* **57** 153
[33] Bustarret E, Ligeon M, Mihalcescu I and Oswald J 1995 *Thin Solid Films* **255** 234
[34] Metropolis N, Rosenbluth A W, Rosenbluth M N, Teller A H and Teller E 1953 *J. Chem. Phys.* **21** 1087
[35] Teschke O, Goncalves M C and Galembeck F 1993 *Appl. Phys. Lett.* **63** 1348
[36] Noolandi J, Hong K M and Street R A 1980 *Solid State Commun.* **34** 45
[37] Street R A 1981 *Adv. Phys.* **30** 593
[38] Silver M, Schoenherr G and Bässler H 1982 *Phys. Rev. Lett.* **48** 352
[39] Tamor M A 1987 *Phys. Rev.* B **35** 5729
[40] Ries B, Bässler H, Grünewald M and Movaghar B 1988 *Phys. Rev.* B **37** 5508
[41] Sinai Y 1982 *Theor. Prob. Appl.* **27** 256
[42] Roman H E, Schwartz M, Bunde A and Havlin S 1988 *Europhys. Lett.* **7** 389
[43] Bunde A and Havlin S (ed) 1991 *Fractals and Disordered Systems* (Heidelberg: Springer)
[44] Ceschini M and Pavesi L 1995 *Proc. 22nd Int. Conf. on the Physics of Semiconductors* ed D J Lockwood (Singapore: World Scientific) p 2165
[45] Yamada M, Takazawa A and Tamura T 1992 *Japan. J. Appl. Phys.* **31** L1451
[46] Tessler L R, Alvarez F and Teschke O 1993 *Appl. Phys. Lett.* **62** 2381
[47] Pavesi L 1995 Luminescence of porous and amorphous hydrogenated silicon: analogies and differences *Amorphous Hydrogenated Silicon, Solid State Phenomena: part B. Diffusion and Defect Data* (Zürich: Scitec)
[48] Wilson W L, Szajowski P F and Brus L E 1993 *Science* **262** 1242

[49] Suemoto T, Tanaka K and Nakajima A 1994 *Phys. Rev.* B **49** 11 005
[50] Sawada S, Hamada N and Ookubo N 1994 *Phys. Rev.* B **49** 5236
[51] ‘t Hooft G W, Kessner Y A R R, Rikken G L J A and Venhuizen A H J 1992 *Appl. Phys. Lett.* **61** 2344
[52] Kanemitsu Y, Uto H, Masumoto Y and Maeda Y 1992 *Appl. Phys. Lett.* **61** 2187
[53] Ben-Chorin M, Moller F and Koch F 1993 *J. Lumin.* **57** 19
Ben-Chorin M, Moller F, Koch F, Schirmacher W and Eberhard M 1995 *Phys. Rev.* **51** 2199
[54] Kanemitsu Y 1994 *Phys. Rev.* B **49** 16 845
[55] Dissanayake A S, Wen G W, Hein W, Lin J Y and Jiang H X 1995 *Proc. 22nd Int. Conf. on the Physics of Semiconductors* ed D J Lockwood (Singapore: World Scientific) p 1827